# RSC Advances

## RSC Advances

www.rsc.org/advances

ROYAL SOCIETY OF CHEMISTRY

www.rsc.org/advances

# Graphical Abstract

# Tuning Thermal Conductivity of Crystalline Polymer Nanofibers by Interchain Hydrogen Bonding

Lin Zhang,[a] Morgan Ruesch,[a] Xiaoliang Zhang,[b] Zhitong Bai,[a] and Ling Liu[a*]

*[a] Department of Mechanical and Aerospace Engineering, Utah State University, Logan, UT 84322, USA*
*[b] Institute of Mineral Engineering, Division of Materials Science and Engineering, Faculty of Georesources and Materials Engineering, Rheinisch-Westfaelische Technische Hochschule (RWTH Aachen University), 52064 Aachen, Germany.*

Interchain hydrogen bonds enhance thermal conduction in crystalline polymer nanofibers by confining torsional motion of polymer chains and by increasing the group velocity of phonons.

[*] Corresponding Author; Email: ling.liu@usu.edu

# Journal Name

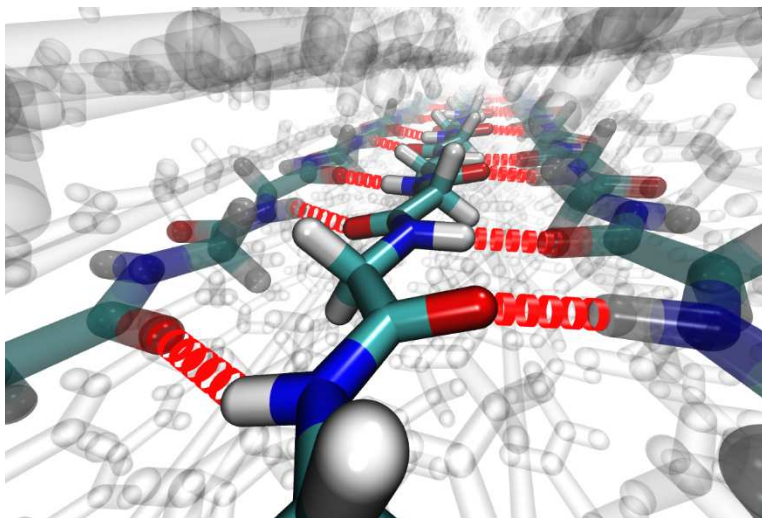## ARTICLE

# Tuning Thermal Conductivity of Crystalline Polymer Nanofibers by Interchain Hydrogen Bonding

Lin Zhang,[a] Morgan Ruesch,[a] Xiaoliang Zhang,[b] Zhitong Bai,[a] and Ling Liu[a*]

Polymers are widely used but they suffer from an apparent bottleneck of inefficient thermal conduction. Here, using non-equilibrium molecular dynamics, we demonstrate that hydrogen-bonded crystalline polymer nanofibers may have thermal conductivities 1-2 orders of magnitude higher than that of engineering polymers. Interchain hydrogen bonds serve as "soft grips" to restrict the torsional motion of polymer chains, leading to enhanced thermal conductivities. The degree of enhancement can be tuned by changing the density of hydrogen bonds, and the number of chains comprising the polymer nanofiber/nanosheet. Further analysis of the dihedral distribution and the phonon dispersion curves attribute such phenomena to the unique effects of hydrogen bonds in confining structural disorder and facilitating phonon transport. The study suggests an important way to tune the thermal conductivity of crystalline polymers.

## 1. Introduction

Polymers are key materials in many engineering technologies for their low mass density, high corrosion resistance, excellent manufacturability, and low costs.[1] Despite the many advantages, the material suffers from an apparent bottleneck. The thermal conductivities of most bulk polymers are only 0.1-1 W/Km,[2] making them inferior to metals and ceramics for applications demanding efficient thermal management. In the meanwhile, however, single polyethylene chains have been reported to be highly conducting with a thermal conductivity of 350 W/m K.[3] The drastic difference underscores the significant influences of molecular structure on the thermal conductivities of polymers, in which hydrogen bond may play a key role.

Fundamentally, the thermal conductivity of polymers is governed by factors including chain morphology, alignment, and the interchain atomistic interactions. For standalone polyethylene chains, nonstraight morphologies including waviness and torsion negatively impact the along-chain thermal conduction.[4] When multiple chains form a nanofiber or a bulk material, chain alignment becomes critical. An ultra-drawn polyethylene nanofiber has demonstrated a high thermal conductivity of 104 W/Km, mainly due to the enhanced phonon transport in mechanically aligned polymer chains.[5] In addition to chain alignment, the strength of the interchain atomistic interaction also influences thermal transport profoundly.[6] In general, thermal conductivity is reduced by weak van der Waals (vdW) interactions, as evidenced in the studies of carbon nanotube bundles,[7] few-layer graphene,[8,9] and polyethylene nanofibers.[10]

10-100 times stronger than the vdW interaction,[11] the hydrogen bonding in polymers can enhance existing thermal pathways and/or create new ones to more efficiently conduct heat. In a recent experimental work, two polymers, i.e. poly(N-acryloyl piperidine) and poly(acrylic acid), were mixed to form a blend in which the interchain hydrogen bonds exerted forces to hold the polymer chains, improving both the interchain and intra-chain heat transfer. Due to this effect, the thermal conductivity of the blend was measured to be 1.5 W/Km, an order of magnitude higher than that of the constituting polymers, i.e. 0.19 and 0.22 W/Km.[12] The experimental study is consistent with our computational work on protein β-sheets. Different from bundled carbon nanotubes and few-layer graphene, β-sheets showed increased thermal conductivities when formed by more constituting units (i.e. β-strands).[13,14] The unusual trend was attributed to the interchain hydrogen bonds, which blueshift and broaden the low-frequency phonon bands leading to enhanced thermal conduction. Similar effects have also been demonstrated in α-helices, where hydrogen bonds create new thermal pathways to enhance thermal diffusion.[15]

Inspired by these findings, hydrogen bond engineering has opened a new avenue to tune the thermal properties of polymers. Nevertheless, a fundamental understanding of the effects of hydrogen bond location, density, and orientation is still lacking. In this work, we use crystalline nylon as a model material to investigate the effects of hydrogen bond density on the nanoscale thermal transport process. We choose nylon because its amide groups (-NH-CO-) can facilitate the formation of hydrogen bonds between the neighboring chains [Figure 1(a)], leading to stable crystalline structures.[16] The non-equilibrium molecular dynamics study will allow us to reveal how thermal conductivity is correlated with the density of hydrogen bonds, and how phonon transport is facilitated by the interchain hydrogen bonds. The results are expected to guide a rational design of hydrogen-bonded crystalline polymers for improved thermal conductivities.

[a.] *Department of Mechanical and Aerospace Engineering, Utah State University, Logan, UT 84322, USA.*
[b.] *Institute of Mineral Engineering, Division of Materials Science and Engineering, Faculty of Georesources and Materials Engineering, Rheinisch-Westfaelische Technische Hochschule (RWTH Aachen University), 52064 Aachen, Germany.*
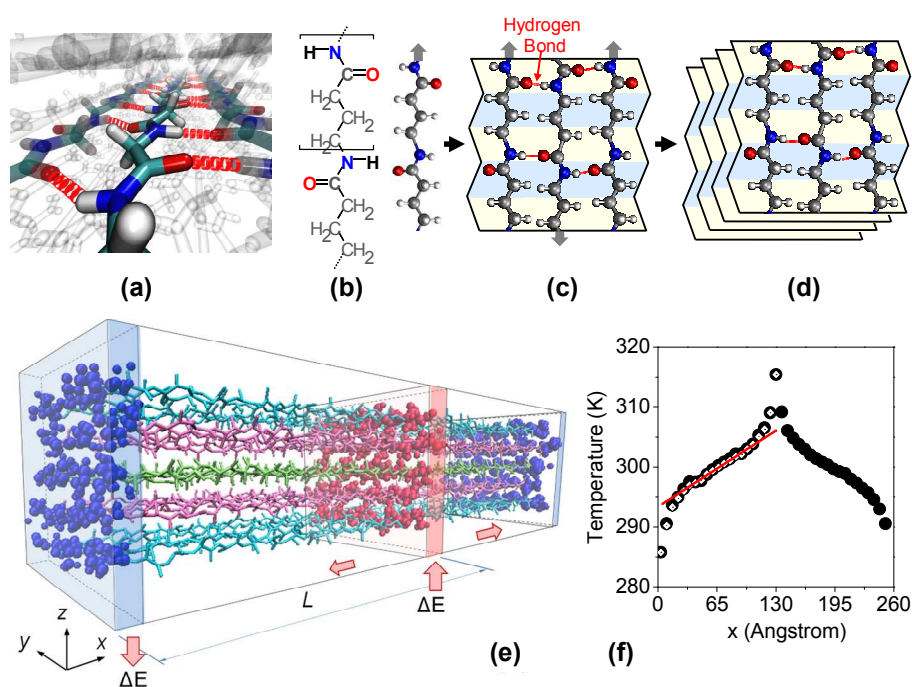\* Email: ling.liu@usu.edu

Figure 1. (a) Illustration of hydrogen bonds in crystalline polymers. (b) Molecular structure of an extended polymer chain of nylon 4. Silver, blue, white, and red spheres represent the carbon, nitrogen, hydrogen, and oxygen atoms, respectively. (c) Multiple such chains are interlocked by hydrogen bonds to form a crystalline nanosheet. (d) Multiple such nanosheets stack to form a nylon crystal. Arrows in (b) and (c) indicate the directions of the polymer chains defined from NH to CO. Chains with alternating directions indicate the anti-parallel arrangement leading to the α-form crystal. (e) Computational model of a crystalline nylon nanofiber. Non-equilibrium molecular dynamics simulation is performed to induce a heat flux from the heat source (red slab) to the heat sink (blue slab). (f) An example temperature profile (solid spheres) along the direction of heat flux (x-direction). Temperature gradient is evaluated by linear regression of the linear portion (red line), which further leads to the thermal conductivity.

## 2. Models and Methods

### 2.1. Models

Previous studies have showed that interchain interactions are critical to determining the thermal properties of polymers. In crystalline nylon, hydrogen bonding dominates the interaction within the polymer sheets, while vdW forces govern the interaction between the sheets. To reveal the effects of both factors on the thermal conduction process, we performed a systematic study using nylon nanofibers of different sizes, i.e. nylon-$n$-$p$-$m$-$q$, where $n$ is the number of carbon atoms in each repeat unit, $p$ is the number of repeat units per chain, $m$ is the number of chains per sheet, and $q$ is the number of sheets in the nanofiber [Figure 1(e)]. Figure 1(b-d) illustrates the molecular structure of crystalline nylon. As a polyamide, nylon consists of numerous copies of [-NH-CO-(CH$_2$)$_{n-1}$-], where $n$ denotes the number of carbon atoms in each repeat unit. Different numbers of $n$ lead to different nylon materials. For example, $n = 4$ gives nylon 4 which has the molecular structure [-NH-CO-(CH$_2$)$_3$-] [Figure 1(b)]. When many of such polymer chains are bundled, the chains are interlocked by hydrogen bonds to form crystalline sheets [Figure 1(c)], which may further stack to form crystals [Figure 1(d)]. Here, we note that nylon chains are directional (from NH to CO). Arranging the chains in the anti-parallel and parallel patterns would lead to different forms of the material (i.e. the α and γ forms). This work is focused on the α-form nylon

because it is more stable and more conducting.[13,14,17]

### 2.2. Structural relaxation

The molecular structures of the nanofibers were relaxed by minimization with the conjugate gradient method, followed by molecular dynamics equilibration of 5 ns at 300 K using the NVT ensemble and the time step of 1 fs. All simulations were performed using LAMMPS[18] with the OPLSAA force field.[19] OPLSAA has been shown by a previous comparative study to be the most effective force field in describing the hydrogen bonding energy and in maintaining the stability of several hydrogen-bonded molecular complexes.[20] All force field parameters used in our simulations can be found in ESI, Section 1. Particle-particle particle mesh method (PPPM) was adopted to account for the long-range Coulomb's interactions. Periodic boundary condition was applied along all the three directions. Large unit cell sizes were assumed along the transverses directions to minimize the artificial interactions between the images of a molecular structure. Nose-Hoover thermostat was employed to maintain temperature at specified values.

### 2.3. Non-Equilibrium molecular dynamics

To apply the method,[21] it is required that the system contains two copies of the nanofiber to be analyzed, i.e. the original structure and an image, both physically connected and symmetric about their center along the direction of intended heat flow (x-direction in this study). The entire system was then divided into $N$ slabs along the x-direction. A heat flux was generated by continuously swapping the

**ARTICLE**

velocities of the "coldest" atoms (with the lowest kinetic energy) in the "heat source" slab and the "hottest" atoms (with the highest kinetic energy) in the "heat sink" slab. During this velocity-swap process, a virtual elastic collision model[22] was employed to ensure the conservation of both system energy and momentum equilibrium. By adjusting the swapping frequency, the temperatures of the hot and cold regions were controlled to be approximately 300±15 K in all cases. Due to the symmetric nature of the system, the characteristic length, $L$, of the model equals to half the system length. The simulations were performed using the NVE ensemble. The time step was set to be 0.5 fs, small enough to capture the dynamics of the hydrogen bonds. We note that, to reach the equilibrium state where a stable temperature profile is formed, models of different sizes would need different lengths of simulations (10~30 ns). Only after equilibrium can we calculate the temperature in the slabs (based on the production run of 10~30 ns) and calculate the thermal conductivity.

### 2.4. Calculation of thermal conductivity

Each non-equilibrium molecular dynamics simulation led to a temperature profile similar to that shown in Figure 1(f). The temperature profile is nonlinear due to the perturbation caused by the artificial velocity swapping. An average was taken between the temperature profiles to the left and right of the heat source. Line regression was then calculated to obtain the temperature gradient. On the other hand, the induced heat flux was evaluated by $J=\Delta E/2tA$, where $t$ denotes the time interval between two swaps, $\Delta E$ is the averaged kinetic energy transferred per swap, $A$ is the cross-sectional area of the material, and the coefficient "2" reflects the two symmetric heat transport paths from the hot slab to the cold slab. The value of $A$ was calculated based on the chain-averaged cross-sectional area in the multilayer nanocrystals. Finally by Fourier's law, thermal conductivity was calculated by $\kappa = -J / \frac{dT}{dx}$, where $\frac{dT}{dx}$ is the temperature gradient along the $x$-direction.

### 2.5. Phonon dispersion curves

Phonon dispersion curves were calculated based on the finite displacement method by using the PHONOPY[23] and LAMMPS[18] packages. In the calculation, each unit cell comprised of two repeat units along the chain direction to ensure geometric periodicity. All atoms in the unit cell form a basis. There are 14 atoms in the basis of the single-chain nylon 2, and 28 atoms in the basis of the double-chain nylon 2. In a supercell of 4 unit cells, LAMMPS was used to calculate the pairwise force when one atom was positively or negatively displaced by a small distance along one of the three Cartesian coordinate directions. The derived force values were used to calculate the force constants which form the dynamic matrix. Finally, the phonon dispersion relations were derived from the eigenvalues of the dynamical matrix.

## 3. Results and discussion

### 3.1. Hydrogen bonding-enhanced thermal conductivity

Figure 2(a) demonstrates that indeed, the interchain hydrogen bonds facilitate thermal conduction in crystalline nylon nanosheets. We start from monolayer nanosheets because hydrogen bonding dominates the interchain interaction which allows us to pinpoint its effects on thermal transport. Four types of nylon nanosheets were considered, i.e. nylon 2 (glycine), nylon 4, nylon 8, and nylon 10. For each of them, the number of nylon chains was varied from 2 to 3, 5, 7, and 9. All nanosheets were made to have 20 repeat units along the chain direction. Due to the different numbers of carbon atoms in

Table 1. Length and thermal conductivity of four fully extended nylon chains. Each of them has 20 repeat units along the chain direction.

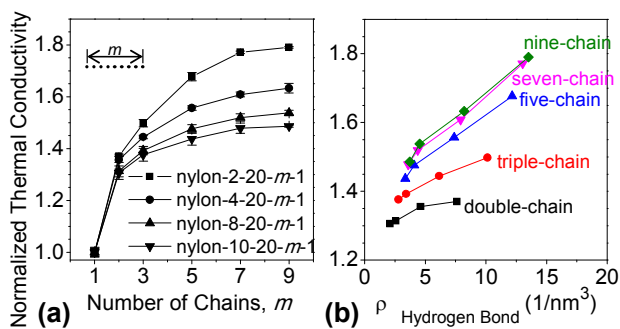|  | nylon 2 | nylon 4 | nylon 8 | nylon 10 |
|---|---|---|---|---|
| Length (nm) | 7.7 | 12.7 | 22.9 | 28 |
| Thermal Conductivity (W/Km) | 5.31 | 5.77 | 6.48 | 7.83 |



**(a)**
**(b)**

Figure 2. (a) Normalized thermal conductivity of 20 nylon nanosheets with different types and different widths (characterized by $m$). The thermal conductivity of each nanosheet is normalized by that of a nylon single chain ($m = 1$) that has the same type. The normalized thermal conductivity provides a means to quantify the change of thermal conductivity caused by hydrogen bonds. (b) Normalized thermal conductivity versus the number density of hydrogen bonds in the nanosheet.

the repeat units, the nylon nanosheets have different lengths (see Table 1 for the lengths of the polymer chains of different types). The thermal conductivity of each nanosheet was then calculated and normalized by that of a single polymer chain of the same type and same length (see Table 1 for the thermal conductivities of the polymer single chains). The normalized thermal conductivity provides a means to quantify the change of thermal conductivity caused by hydrogen bonds. As shown in Figure 2(a), the thermal conductivities of all nylon nanosheets increase with the number of chains. This echoes our previous study on protein β-sheets, both showing positive contributions of hydrogen bonds to the nanoscale thermal transport process.

Furthermore, it is discovered that the degree of enhancement in thermal conductivity is controlled by the density of hydrogen bonds. Figure 2(b) plots the normalized thermal conductivity as a function of the number density of hydrogen bonds in the nanosheet. Five lines are shown, and they correspond to the nanosheets of different widths (or different numbers of chains, $m$). In each line, there are four data points which correspond to the four types of nylon. The type of nylon and the number of chains both determine the density of hydrogen bonds in a nanosheet. Overall, we find that the normalized thermal conductivity (i.e. the degree of enhancement) increases with the density of hydrogen bonds which, again, demonstrate the positive contributions of hydrogen bonds to heat transfer.

It is worth pointing out that the thermal conductivities revealed by our simulations for crystalline nylon nanofibers are much higher than that reported for bulk nylon materials (typically 0.25 W/m K[24]). The different thermal conductivities result from the different structures of these materials. In bulk nylon, polymer chains are randomly oriented with weakly coupled chains, and there are numerous impurities and imperfections. All these factors lead to high
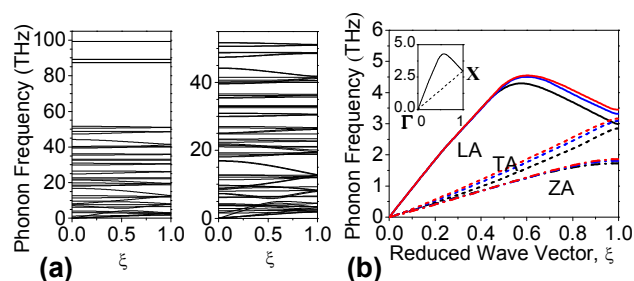
Figure 3. (a) Phonon dispersion curves of nylon2-2-1-1 (left) and nylon2-2-2-1(right). ξ is the reduced wave vector defined to be $q_x/(\pi/a_x)$, where $q_x$ and $a_x$ are the wave vector component and the lattice constant in the $x$ direction, respectively. For nylon2-2-2-1, frequencies higher than 55 THz are truncated for visual clarity. (b) Acoustic phonon branches are compared between nylon2-2-1-1 (black), nylon2-2-2-1 (blue), and nylon2-2-3-1 (red). LA, TA, and ZA refer to the longitudinal, transverse, and out-of plane acoustic phonon branches, respectively. The slope of these phonon dispersion curves indicates the group velocity. Inset of (b) shows the definition of the average group velocity, i.e. the slope of a line connecting the origin (Γ) and the point X (the intersection between the phonon branch and the line with ξ = 1).

phonon scattering, short phonon mean free path, and hence low thermal conductivities. In the crystalline nylon nanofibers, however, the polymer chains are highly oriented and defects are reduced, all of which contribute to the improved thermal conduction. Such high thermal conductivities of polymer nanofibers have been experimentally demonstrated using nylon 11 nanofibers with the thermal conductivities measured to be about 1.6 W/m K.[25] Our work presented in this paper provides a systematic fundamental understanding of why thermal conduction is improved in the nylon polymer nanofibers, and how hydrogen bonds contribute to this improvement.

### 3.2. Hydrogen bonding increases phonon group velocity

To reveal the phonon physics, dispersion curves were generated for selected crystalline nylon 2 nanosheets using the finite displacement method. Figure 3(a) plots the phonon dispersion curves of a single-chain and a double-chain nylon 2 nanosheets. It is readily seen that, phonons at low frequencies are predominantly excited by the Boltzmann distribution; and most optical phonon branches, especially those with higher frequencies, have a group velocity of zero. Therefore, it is confirmed that heat is mainly transferred by acoustic phonons. To further understand the effects of hydrogen bonds, Figure 3(b) plots the three acoustic phonon branches for the single-, double-, and triple-chain nanosheets, respectively. The slope of each phonon branch indicates the group velocity at a specific ξ. The slope of a line connecting Γ and X in Figure 3(b) defines the average group velocity.

From the single chain to the hydrogen-bonded triple-chain nanosheet, acoustic phonons of all polarization branches demonstrate a blueshift owing to the increasing hydrogen bonds. The blueshift in frequency is directly linked with the increase of group velocities. Specifically, hydrogen bonds increase the group velocity of longitudinal acoustic (LA) phonons when ξ falls in the range of 0.23-0.38; for out-of-plane acoustic (ZA) and transverse acoustic(TA) phonons, however, hydrogen bonds increase the group velocity almost throughout the entire first Brillouin zone. Therefore, the confinement of chains in a hydrogen bonded environment can, either partially or entirely, increase the group velocities of acoustic phonons in all polarization branches. This partially explains the
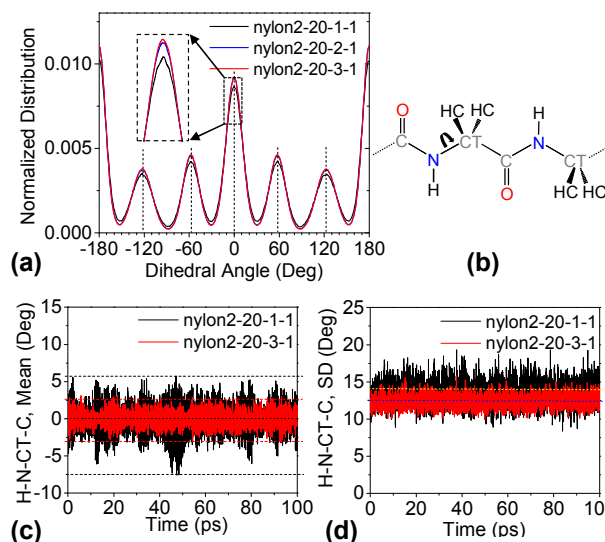


Figure 4. (a) Normalized distribution of all dihedrals in the nylon2-20-*m*-1 nanosheets where *m* is 1, 2, and 3, respectively. (b) The H-N-CT-C dihedral. (c) The mean of all H-N-CT-C dihedrals versus time. Dashed lines show the average, upper bound, and lower bound of the dihedrals. Inset defines the H-N-CT-C dihedral as the torsional angle between the H-N-CT plane and the N-CT-C plane. (d) The standard deviation of all H-N-CT-C dihedrals versus time. Dashed lines show the average.

enhanced thermal conductivities of the hydrogen-bonded crystalline polymers. By phonon Boltzmann transport equation,[26] the thermal conductivity of a one-dimensional system $k_x = C_v \cdot v_x \cdot \Lambda$, where $C_v$ is the heat capacity, $v_x$ is the representative group velocity of phonons, and Λ is the phonon mean free path. Higher average group velocity in hydrogen-bonded polymers contributes to enhancing the thermal conductivities.

### 3.3. Hydrogen bonding improves inter-chain lattice ordering

In addition to increasing phonon transport velocity, hydrogen bonds also improve structural ordering which reduces phonon scattering. The importance of structural ordering to efficient thermal conduction has been demonstrated in many previous studies.[4,27] For polymers (even for those with well aligned chains), there is an important factor that can cause structural disorder and thereby obstruct thermal conduction – torsion of the chains. In a recent computational study of polyethylene nanofibers [4], Zhang et al. tuned the torsion of chains by adjusting the dihedral parameters in the force field; the polymers with restricted torsional motion were found to have higher thermal conductivities. Using the same approach, similar conclusions have been reached for crystalline nylon polymers (see ESI, Figure S1). It is hypothesized that, in hydrogen-bonded polymer nanofibers, the interchain hydrogen bonds can confine torsional motion, thereby improving thermal conductivity.

To demonstrate the critical role of hydrogen bonds in improving structural ordering, we statistically analyzed the dihedral distribution in the single-chain, double-chain, and triple-chain nylon 2 nanosheets. Dihedral A-B-C-D is defined by four successively chemical bonded atoms A, B, C, and D; and it describes the torsional angle between the A-B-C plane and B-C-D plane about the axis connecting B and C. There are 12 types of dihedrals in nylon 2. Figure 4(a) plots the angle distribution of all dihedrals for each of the three nanosheets, respectively. There are seven peaks identified,
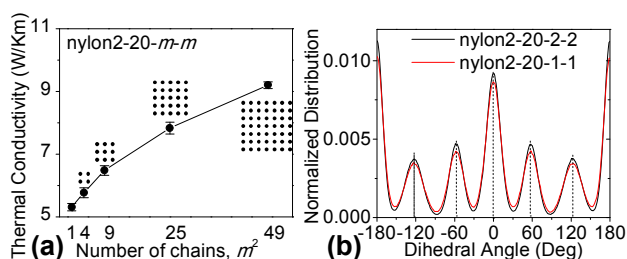
**ARTICLE**



Figure 5. (a) Thermal conductivity of multilayer nylon 2 nanofibers, nylon2-20-*m-m*, where *m* is 1, 2, 3, 5, and 7. Here, thermal conductivity is plotted against the number of chains to show the dependence of thermal conductivity on the cross-sectional area of the polymer nanofibers. (b) Normalized dihedral distribution of the nylon2-20-2-2 nanofiber and the nylon2-20-1-1 single chain.

centered about ±180º, ±122.7º, ±57.8º, and 0º. The dihedrals centered about ±180º are C-N-CT-C, CT-N-C-CT, N-C-CT-N, and H-N-C-O which mainly represent the torsion of the main chain; the dihedrals centered about ±122.7º are H-N-CT-HC and O-C-CT-HC which describe the torsion involving hydrogen bond donors (H) and acceptors (O) with respect to HC; the dihedrals centered about ±57.8º are C-N-CT-HC and N-C-CT-HC; the dihedrals centered about 0º are H-N-CT-C, H-N-CT-N, O-C-CT-N, and CT-N-C-O which also characterize the torsion involving hydrogen bond donors and acceptors about the main chain. The angle distribution of each of these dihedrals can be found in ESI, Figure S2.

Comparing the dihedral distributions, we find that the hydrogen-bonded triple-chain nanosheet has the highest and sharpest peaks among the three nylon 2 nanosheets under investigation. In other words, the dihedrals in the triple-chain nanosheet are less deviated from their equilibrium values, leading to less twisted and more ordered chains. In such crystalline polymers, the hydrogen bond donors and acceptors have higher probabilities to reside on the same plane of the main chain atoms; and the rotation of all side atoms about the main chain is strongly restricted. All these factors contribute to an improved interchain lattice order of the polymers, leading to enhanced thermal conductivities.

More statistical analysis was performed to further demonstrate the variation of the various dihedrals over time. At each time step, all dihedral angles of the same type were averaged to give a mean value; and the standard deviation (SD) was evaluated as well to quantify the fluctuation. Both the mean and the standard deviation are shown in Figure 4(c-d) as functions of time for the H-N-CT-C dihedral [Figure 4(b)]. The data of other 11 dihedrals can be found in the ESI, Figures S3-S4. Apparently, all history curves in Figure 4(c) fluctuate about 0º which is the equilibrium angle of the H-N-CT-C dihedral. Due to the hydrogen bonds that restrict torsion, the triple-chain nylon 2 nanosheet demonstrates the most stable H-N-CT-C dihedral (with the least deviation from 0º). All these results, again, demonstrate the positive effects of hydrogen bonds in maintaining highly ordered crystalline polymers for efficient thermal conduction.

### 3.4. Coupled effects of inter-sheet vdW interaction and intra-sheet hydrogen bonding

The above analysis is focused on polymer nanosheets to reveal the critical contributions of hydrogen bonds to the nanoscale thermal transport. As many of such nanosheets stack to form nanofibers, the vdW interaction takes effect and dominates the interchain interactions between the nanosheets. While hydrogen bonding has been shown to facilitate thermal conduction in crystalline polymer nanosheets, the vdW interaction is known to be a factor obstructing

thermal conduction in many other materials[8,28,29]. As both of them compete in the crystalline nanofibers, which one will win? To answer this question, we computed the thermal conductivities of four nylon 2 nanofibers, i.e. nylon2-20-*m-m* with *m* varied from 2 to 3, 5, and 7, and the results are shown in Figure 5(a). As the nanofiber grows in both transverse directions, the thermal conductivity keeps increasing with a tendency to converge. The main contributor to the increased thermal conductivity is, again, the intra-sheet hydrogen bonds. Comparing the dihedral distributions of the single chain and the 2×2 nanofiber in Figure 5(b), we find that the 2×2 nanofiber has sharper peaks implying more ordered structure.

It is worthwhile to further compare Figure 5(a) with Figure 2(a). The former shows the variation of thermal conductivity from 1D to 3D, while the latter shows the variation of thermal conductivity from 1D to 2D. Structurally, in the 2D sheets, the polymer chains are bundled by hydrogen bonds; in the 3D fibers, the sheets stack as facilitated by the inter-sheet vdW interaction. In general, it is found that the inter-sheet vdW interaction in the 3D nanofibers adversely affects the improvement caused by the intra-sheet hydrogen bonds. However, due to the prominent effects of hydrogen bonds, the thermal conductivity still increases as the nylon nanofibers grow in transverse directions. This trend is opposite to that previously shown for the polyethylene nanofibers; due to the nonexistence of hydrogen bonds in polyethylene, the thermal conductivity of the polyethylene nanofibers was shown to decrease from 1D to 2D and from 2D to 3D.[10]

## 4. Conclusions

In summary, we have demonstrated that the interchain hydrogen bonds in crystalline polymers serve as "soft grips" to restrict the torsional motion of polymer chains, leading to enhanced thermal conductivities. Higher thermal conductivities can be achieved by increasing the density of hydrogen bonds, or by increasing the number of chains comprising the polymer nanofibers/nanosheets. This is opposite to the effects of the vdW interaction. Many previous studies have shown that the vdW interaction obstructs heat transfer in carbon nanostructures; as a bundled/layered structure comprises of more and more carbon nanotubes or graphene layers, thermal conductivity decreases.[8,28] The unique contribution of hydrogen bonding to heat transfer is linked with its profound effects on the structural ordering and phonon transport. Suggested by the analysis of the dihedral distribution and phonon dispersion, the hydrogen bonds in crystalline polymers restrict torsion, blueshift acoustic phonon branches, and increase the averages group velocities of phonons. Such effects of hydrogen bonds can be applied to rationally design crystalline polymers for improved thermal conductivities.

## Notes and references

1.  M. Chanda and S. K. Roy, *Plastics Technology Handbook*, CRC Press, 2006.
2.  C. L. Choy, *Polymer*, 1977, **18**, 984-1004.
3.  A. Henry and G. Chen, *Phys Rev Lett*, 2008, **101**.
4.  T. Zhang and T. F. Luo, *J Appl Phys*, 2012, **112**.

5.  S. Shen, A. Henry, J. Tong, R. T. Zheng and G. Chen, *Nat Nanotechnol*, 2010, **5**, 251-255.
6.  T. Sun, J. X. Wang and W. Kang, *Nanoscale*, 2013, **5**, 128-133.
7.  J. Hone, B. Batlogg, Z. Benes, A. T. Johnson and J. E. Fischer, *Science*, 2000, **289**, 1730-1733.
8.  S. Ghosh, W. Z. Bao, D. L. Nika, S. Subrina, E. P. Pokatilov, C. N. Lau and A. A. Balandin, *Nat Mater*, 2010, **9**, 555-558.
9.  D. Singh, J. Y. Murthy and T. S. Fisher, *J Appl Phys*, 2011, **110**, 044317.
10.  A. Henry, G. Chen, S. J. Plimpton and A. Thompson, *Phys Rev B*, 2010, **82**.
11.  T. Steiner, *Angewandte Chemie International Edition*, 2002, **41**, 48-76.
12.  G.-H. Kim, D. Lee, A. Shanker, L. Shao, M. S. Kwon, D. Gidley, J. Kim and K. P. Pipe, *Nat Mater*, 2015, **14**, 295-300.
13.  L. Zhang, T. Chen, H. Ban and L. Liu, *Nanoscale*, 2014, **6**, 7786-7791.
14.  L. Zhang, Z. Bai, H. Ban and L. Liu, *Phys Chem Chem Phys*, 2015, DOI: 10.1039/C5CP04621A.
15.  G. Miño, R. Barriga and G. Gutierrez, *The Journal of Physical Chemistry B*, 2014, **118**, 10025-10034.
16.  S. Dasgupta, W. B. Hammond and W. A. Goddard, *J Am Chem Soc*, 1996, **118**, 12291-12301.
17.  Y. Y. Li and W. A. Goddard, *Macromolecules*, 2002, **35**, 8440-8455.
18.  S. Plimpton, *J Comput Phys*, 1995, **117**, 1-19.
19.  W. Damm, A. Frontera, J. TiradoRives and W. L. Jorgensen, *J Comput Chem*, 1997, **18**, 1955-1970.
20.  R. S. Paton and J. M. Goodman, *J Chem Inf Model*, 2009, **49**, 944-955.
21.  F. Muller-Plathe, *J Chem Phys*, 1997, **106**, 6082-6085.
22.  C. Nieto-Draghi and J. B. Avalos, *Mol Phys*, 2003, **101**, 2303-2307.
23.  A. Togo and I. Tanaka, *Scripta Mater*, 2015, **108**, 1-5.
24.  A. L. Moore, A. T. Cummings, J. M. Jensen, L. Shi and J. H. Koo, *Journal of Heat Transfer*, 2009, **131**, 091602-091602.
25.  Z. X. Zhong, M. C. Wingert, J. Strzalka, H. H. Wang, T. Sun, J. Wang, R. K. Chen and Z. Jiang, *Nanoscale*, 2014, **6**, 8283-8291.
26.  G. Chen, *Nanoscale energy transfer and conversion*, Oxford University Press, 2005.
27.  J. Liu and R. G. Yang, *Phys Rev B*, 2012, **86**.
28.  M. T. Pettes and L. Shi, *Adv Funct Mater*, 2009, **19**, 3918-3925.
29.  Z. D. Han and A. Fina, *Prog Polym Sci*, 2011, **36**, 914-944.